Microbial community abundance and biomass along a 180° transect in the equatorial Pacific during an El Niño-Southern Oscillation cold phase

Susan L. Brown and Michael R. Landry
Department of Oceanography, University of Hawaii at Manoa, Honolulu, Hawaii, USA

Jacques Neveux
Observatoire Océanologique de Banyuls, Laboratoire Arago (UMR 7621), Banyuls sur Mer, France

Cécile Dupouy
Laboratoire d'Océanographie Dynamique et de Climatologie (LODYC), Institut de Recherche pour le Développment (IRD), Université Pierre et Marie Curie, Paris, France

Received 29 January 2001; revised 17 January 2003; accepted 25 April 2003; published 16 December 2003.

[1] As part of the French Joint Global Ocean Flux Study Etude du Broutage en Zone Equatoriale program, we investigated the distributions of microorganisms (bacteria and protists <200 μm) in the upper 120 m of the equatorial Pacific from 8°S to 8°N, along 180°. Population distributions, determined by a combination of flow cytometry, microscopy and spectrofluorometry, were closely related to physical features across the study site. Phytoplankton biomass, ranging from 1.2 to 34.2 μg C L^{-1} and averaging 15.5 μg C L^{-1}, was most enhanced in the divergence zone. Carbon to chlorophyll ratios were also enhanced in the divergence zone and showed distinct latitudinal variations. Heterotrophic biomass, excluding ciliates, was patchy across the area, ranging from 5 to 36 μg C L^{-1} and averaging 13 μg C L^{-1}. Prokaryotic species (*Prochlorococcus* spp., *Synechococcus* spp., and heterotrophic bacteria) showed similar patterns of abundance, with the main feature being their distributional asymmetry to the south of the equator. Both autotrophic and heterotrophic biomass were enriched in the convergent zone at 4°–5°N between the South Equatorial Current and the North Equatorial Counter Current. Heterotrophic biomass exceeded phytoplankton biomass in the more nutrient-impoverished waters to the north and in the branch of a tropical instability wave eddy. Microplankton represented only a small portion of the total autotrophic carbon and was comprised mostly of dinoflagellates. Large species dominated the relatively modest diatom biomass. Food web interactions and biogeochemical fluxes in the central equatorial Pacific may be significantly influenced by temporal and spatial variability of the microbial community associated with physical features of the region. *INDEX TERMS:* 4231 Oceanography: General: Equatorial oceanography; 4223 Oceanography: General: Descriptive and regional oceanography; 4815 Oceanography: Biological and Chemical: Ecosystems, structure and dynamics; 4840 Oceanography: Biological and Chemical: Microbiology; *KEYWORDS:* microbial community structure, plankton, equatorial Pacific

Citation: Brown, S. L., M. R. Landry, J. Neveux, and C. Dupouy, Microbial community abundance and biomass along a 180° transect in the equatorial Pacific during an El Niño-Southern Oscillation cold phase, *J. Geophys. Res.*, *108*(C12), 8139, doi:10.1029/2001JC000817, 2003.

1. Introduction

[2] Recent advances in technology (e.g., flow cytometry) and recognition of the "microbial loop" have stimulated interest in the biomass and diversity of the microbial community (biota <200 μm). Components of the microbial community, namely bacteria and protists, range in size over three orders of magnitude, belong to at least three different kingdoms and represent numerous trophic modes. The microbial community also comprises the base of the food web; hence its structure exerts strong influences on energy flows to higher trophic levels and biogeochemical fluxes. In addition to quantification of the microbial community, an essential part of understanding the base of the food web is identifying the factors that influence microbial biomass and structure, both of which are necessary for predictive models.

0148-0227/03/2001JC000817$09.00

[3] Community structure can vary on seasonal, annual and decadal timescales, as well as regional scales, mesoscales, and fine spatial scales. Multiple factors determine microbial community structure, but the resulting assemblages principally reflect the net effects of physical forcing, which affects the inputs and distributions of "new" nutrients and trace elements, and grazing impacts. The upwelling zone of the equatorial Pacific represents a diverse physical region and a major environmental gradient across the tropical open ocean. Our goal in this study was to assess how microbial populations and biomass varied across gradients and physical features in the equatorial Pacific. In the Etude du Broutage en Zone Equatoriale (EBENE) program, a quantitative assessment of phytoplankton and microzooplankton stocks and functional groups was the foundation for evaluating the balance between phytoplankton growth and zooplankton grazing processes. Here we present a comprehensive synthesis of the heterotrophic and autotrophic components of the protist community, within the context of food web structure and the physiochemical environment in a cross equatorial transect during the ENSO cold phase of 1996.

2. Materials and Methods

[4] The distributions, abundances and biomass of microorganisms (bacteria and protists <200 μm) were estimated by three complementary methods: flow cytometry, image-enhanced microscopy and spectrofluorometry. As part of the French Joint Global Ocean Flux Study (JGOFS) EBENE cruise, stations were positioned every degree of latitude along a north-south transect from 8°S to 8°N, 180° (21 October to 20 November 1996). Subsamples for microorganisms were taken in the upper 120 m, at 6–8 depths per station, from Niskin bottles attached to a CTD rosette system. Data were grouped in to two different depth strata, 0–50 m and 50–100 m, corresponding to the upper two depth strata of complementary plankton tows [*Le Borgne et al.*, 2003]. Subsamples were analyzed as described below.

2.1. Flow Cytometry

[5] Samples (1 mL) for flow cytometric (FCM) analysis were preserved in cryogenic tubes with paraformaldehyde (0.5% final concentration) and frozen in liquid nitrogen. FCM samples were subsequently thawed and stained with Hoechst 33342 (0.8-μg mL^{-1} final concentration) for 30 min before analysis of microbial populations [*Monger and Landry*, 1993]. Subsamples of 100 μL were enumerated on a Coulter EPICS 753 flow cytometer equipped with dual argon lasers and MSDS II automatic sampling. The lasers were aligned colinearly with the first laser tuned to the UV range to excite Hoechst-stained DNA. The blue fluorescence from the DNA stain was used to distinguish cells from nonliving particulate matter. The second laser was tuned to 488 nm at 1.0 W to excite the chlorophyll *a* and phycoerythrin of autotrophic cells. *Prochlorococcus* and *Synechococcus* populations were distinguished from one another by differences in light scatter and fluorescence emission. Heterotrophic bacteria were distinguished by the presence of DNA-stain and the absence of red chlorophyll fluorescence (680 nm ± 40 nm). The remaining chlorophyll-bearing organisms were grouped as small photosynthetic eukaryotes (≤8-μm PEUKS), which represented a continuous size spectrum of cells [*Olson et al.*, 1990a]. All FCM samples were spiked with a mixture of Polysciences Fluoresbrite YG 0.57- and 0.98-μm visible beads and 0.46-μm UV beads. As a proxy for pigment per cell, cellular red fluorescence of enumerated phytoplankton was normalized to the fluorescence of the standard 0.57-μm beads. The close agreement between FCM-derived red fluorescence per cell and chlorophyll per cell for *Prochlorococcus* populations ($r = 0.978$) and phytoplankton as a whole ($r = 0.932$) is presented by *Landry et al.* [2003, Figure 5]. Cell abundances of heterotrophic bacteria, *Prochlorococcus* spp. and *Synechococcus* spp. were converted to biomass using conversion factors of 11, 32, and 101 fg C $cell^{-1}$, respectively [*Garrison et al.*, 2000]. Cell abundances of PEUKS were converted to biomass using latitude-specific conversion factors as described below.

2.2. Microscopy

[6] Aliquots of 50 and 250 mL were collected for image-enhanced epifluorescent microscopy. Subsamples of 50 mL were preserved with 0.5% paraformaldehyde and stained with 25 μL of proflavin (0.33% w/v). Subsamples of 250 mL were preserved with 250 μL of alkaline Lugol's solution followed by 2 mL of formalin and 125 μL of sodium thiosulfate (modified protocol from *Sherr and Sherr* [1993]); they were then stained with 75 μL of proflavin. Preserved subsamples were slowly (≈5 psi) filtered onto either black 0.6-μm (50 mL) or 8.0-μm (250 mL) Nuclepore filters overlaying 10-μm Millipore backing filters to facilitate even cell distributions. During filtration, the samples were drawn down until approximately 5 mL remained in the filtration tower. Concentrated DAPI (50 μg mL^{-1}) was added and allowed to sit for 30 s before drawing down the remainder of the samples until the filters were dry. Filters were mounted onto glass slides with immersion oil and cover slips. The slides were then frozen and stored in the dark at −70°C.

[7] Thawed slides were analyzed with a color image analysis system. Cells were viewed at either 400X (50-mL aliquots) or 250X (for 250-mL aliquots) with a Zeiss Standard 16 Microscope configured with an epifluorescent kit and 100-W power supply. The microscope was fitted with a C mount and a Zeiss 3 CCD Video Camera and Processor (ZVS-3C75DE). At least 20 random images per slide were captured and downloaded onto an attached computer via a frame grabber and Zeiss Image software. Counting and sizing of cells greater than 1.5 μm in length were automated with Zeiss Image software. Cells were identified and grouped manually. Autotrophic cells >1.5 μm were distinguished from heterotrophic cells by the presence of chlorophyll seen as red fluorescence under illumination with blue light. Length and width measurements were converted to biovolumes (BV; μm^3) by applying appropriate geometric shapes. Cell volume to carbon conversions for both autotrophic and heterotrophic nanoplankton and microplankton were based on modified *Strathmann* [1967] equations for diatoms ($\log_{10}C = 0.76(\log_{10}BV) - 0.352$) and nondiatom phytoplankton ($\log_{10}C = 0.94(\log_{10}BV) - 0.60$) [*Eppley et al.*, 1970].

[8] Slides from all depths and stations were enumerated and measured for grazer biomass (≤8 μm and >8 μm) and

for the biomass of large photosynthetic eukaryotes (>8-μm PEUKS). The average N counted and measured for large volume slides was 68; almost all cells were <100 μm in length and the large majority were <20 μm. Samples with notably large cells were scanned and quantified at a lower magnification (100X) for a more accurate assessment of biomass. Single, rare cells that skewed biomass estimates were not quantified, thus biomass estimates for large cells may be somewhat conservative.

[9] It was not feasible to quantify the smaller autotrophic eukaryotes (1.5–8 μm) in every sample. Instead, samples from 20 m and 80 m at each station were enumerated and measured to evaluate possible changes in biovolume with depth and latitude. On the basis of the modified *Strathmann* [1967] equation, which is based on biovolume, average carbon per cell factors were calculated for the two depths at each station (Figure 1). The differences between latitudes were greater than the differences between depths (paired t test, p value = 0.31, 95% CL). For this reason, the carbon per cell estimates from the 20-m and 80-m samples at each station were averaged and a latitude-specific carbon per cell conversion factor was applied to the FCM abundance estimates of ≤8-μm photosynthetic eukaryotes (PEUKS) at all depths. The average of the carbon per cell conversion factors applied (1.9 pg C cell^{-1}) is very similar to the previously published estimate of 2.1 pg C cell^{-1} for FCM-derived abundances of photosynthetic eukaryotes [*Campbell et al.*, 1994].

2.3. Spectrofluorometry

[10] Seawater samples (500 mL) for chlorophyll pigment analysis were filtered onto 47-mm Whatman GF/F glass fiber filters. Filters were ground with the end of a freshly broken glass stirring rod, extracted in the dark at 4°C for 12 hours in centrifuge tubes containing 5.4 mL of 100% acetone (final concentration ~90% due to water retention by filter) and then centrifuged. Fluorescence properties of the extracts were measured on a Hitachi F4500 spectrofluorometer operating in ratio mode. Slit widths were 5 and 10 nm for excitation and emission, respectively. Fluorescence emission spectra were recorded for each of 31 excitation wavelengths in 3-nm increments from 390 to 480 nm and in 4-nm increments from 615 to 715 nm (26 wavelengths). Pigment concentrations were estimated from the resulting data set of 806 points (31 × 26) according to least squares approximation [*Neveux and Lantoine*, 1993]. The spectrofluorometric method assumes that the sample contains no more than 10 major chlorophyll derivatives: chlorophyll *a*, chlorophyll *b*, chlorophyll *c*, divinyl chlorophyll *a*, divinyl chlorophyll *b*, and the phaeopigments of these five chlorophylls. Chlorophyll *c* is assumed to be a mixture of chlorophylls c_1 and c_2. Detection limits, precision and concerns with the spectrofluorometric method are discussed by *Neveux and Lantoine* [1993] in which 24 wavelength pairs were used for analysis; it should be noted that the more accurate method of 806 wavelengths was used in this analysis. Pigment concentrations from the spectrofluorometric method agreed well with concurrent estimates from high-performance liquid chromatography (HPLC) as presented by *Landry et al.* [2003].

[11] For phycoerythrin (PE) determination, 1–3 L of seawater were filtered onto a 47-mm 0.4-μm polycarbonate

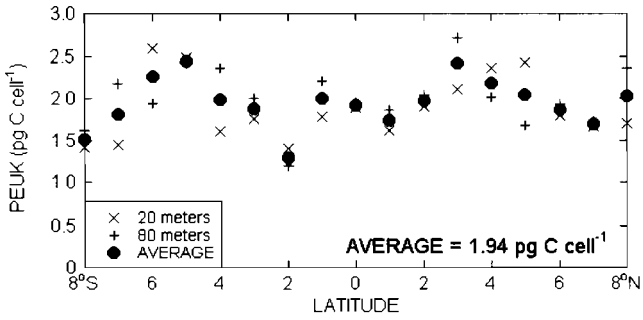

Figure 1. Average carbon (pg) per cell of small (1.5–8 μm) autotrophic eukaryotes at the surface (20 m) and at depth (80 m) and the average for each station across the equatorial transect at 180°.

Nuclepore membrane. Each filter was dipped in a glass tube containing 5 mL of 50% glycerol in phosphate buffer, following the in vivo method of *Wyman* [1992]. After the tubes were vigorously shaken, the cell suspensions were transferred into a 1-cm^2 measuring cuvette. Fluorescence was measured on a Perkin Elmer MPF 66 spectrofluorometer using an OBEY program [*Lantoine and Neveux*, 1997; *Neveux et al.*, 1999]. The program first performed an excitation scan from 450 to 560 nm (emission: 575 nm). Then, depending on the excitation maximum found, the emission was scanned from either 530 to 700 nm (excitation: 495 nm) or 550 to 700 nm (excitation: 530 nm). We calculated PE concentrations using the areas under the fluorescence excitation spectra, the PUB/PEB ratio (495/548 nm ratio) and previously published formulas [*Lantoine and Neveux*, 1997].

2.4. Contour Plots

[12] Contour plots were created by the surface mapping system SURFER Version 7.0. XYZ grid files were generated by Radial Basis Function interpolation. A chosen grid size of 20 × 8 best represented the true values of the data. An anisotropy ratio of 0.2 was applied to account for the large differences in scaling between the X and Y axes. Contour levels were chosen manually to highlight real trends in the data and assure that measured values were accurately represented.

3. Results

3.1. Hydrography

[13] *Eldin and Rodier* [2003, Figures 2 and 3] present a detailed description of the physics and chemistry along the 180° transect during the EBENE study, in addition to results from the two time series stations. We summarize below the features most relevant to the present study.

[14] Surface temperature showed classic wind-driven equatorial upwelling, with colder waters (28.1°C) overlying the equator and extending from 4°S to 5°N, and with warmer waters to the north and south. The top of the thermocline, marked by the 28° isotherm, exceeded 100 m over most of the study site, but shoaled sharply at the equator, nearly reaching the surface. Also noteworthy was a localized deepening of the thermocline at 4°N. The iso-

therms diverged below 100 m at the equator, as typical for the central Pacific region. The 20° isotherm, designating the upper thermocline, was deeper (200 m) to the south of the upwelling region than to the north (120 m) and followed a steeper sloping of isotherms north of 4°N.

[15] Salinity fields showed both horizontal and vertical structure. Salinity was fairly homogenous above the thermocline (35.4 to 35.7) until 5.5°N, where a horizontal gradient down to 150 m marked the boundary to lower-salinity waters (34.5). Below 120 m, a wedge of high-salinity water, presumably a tongue of Tropical Water, intruded from the south. Its intrusion was evident in a distinct vertical gradient between 120–200 m from 8°S northward and ending in a horizontal gradient at the equator.

[16] Upper ocean current fields were determined from ADCP measured zonal and meridional velocities. The South Equatorial Current (SEC) was evident as a westward moving current extending from 5°S to 4°N. Zonal velocities were higher north of the equator, reaching 90 cm s^{-1} versus less than 50 cm s^{-1} south the of the equator. The meridional velocity of the SEC showed a reversal at the equator, from a southward component north of the equator to a northward component south of the equator, resulting in convergence at the site of upwelling. The eastward moving Equatorial Undercurrent (EUC) extended up to 100 m at the equator and was primarily positioned between 2°S and 2°N. Zonal velocities reached 60 cm s^{-1} just above 200 m. Beneath the EUC between 0° and 2°N, the Equatorial Intermediate Current (EIC) was apparent below 200 m as a westward flow reaching 30 cm s^{-1} with a slight southward component. The North Equatorial Counter Current (NECC) was evident as an eastward moving current north of 4°N, extending from the surface down to >300 m and reaching velocities of more than 100 cm s^{-1}. Its eastward flowing southern counterpart, the South Equatorial Counter Current (SECC), was much weaker in zonal velocity, only reaching 10 cm s^{-1}. The SECC was apparent at the surface between 8°S and 5°S in the upper 200 m.

[17] Surface waters overlying the equator were enriched in nitrate (NO_3 > 2 μM) with an asymmetrical distribution from 1°N to 4°S. Concentrations greater than 0.1 μM extended even further from 7°S to 6°N. Similar to isotherms, the divergence of subsurface isolines (>150 m) was apparent under the divergent zone between 2°S and 2°N, reflecting the presence of the EUC. From south to north, nitrate isolines sloped upward with sharpest gradients and highest subsurface concentrations at the northern end of the transect. Phosphate concentrations exhibited a very similar spatial pattern with higher concentrations (PO_4 > 0.3 μM) distributed asymmetrically to the south from 0° to 7°S; however, phosphate concentrations were still greater than 0.1 μM north and south of this region. Subsurface gradients and concentrations mirrored that of nitrate with higher concentrations and sharper gradients to the north.

[18] Surface nitrite concentrations peaked between 1°S and the equator with concentrations >0.2 μM. Highest concentrations of nitrite (>1 μM) were just below 100 m from 8°S to 1°S, centered at 3°–5°S. Additional regions of nitrite enhancement were present below 100 m at 2°N and 5°N. Subsurface ammonia distributions mirrored nitrite and also reached >1 μM south of the equator. However, ammonia surface concentrations were also enhanced (>0.1 μM) from 6°S to 1°S. Enhanced concentrations of silicic acid were centered at the equator and exceeded 2 μM.

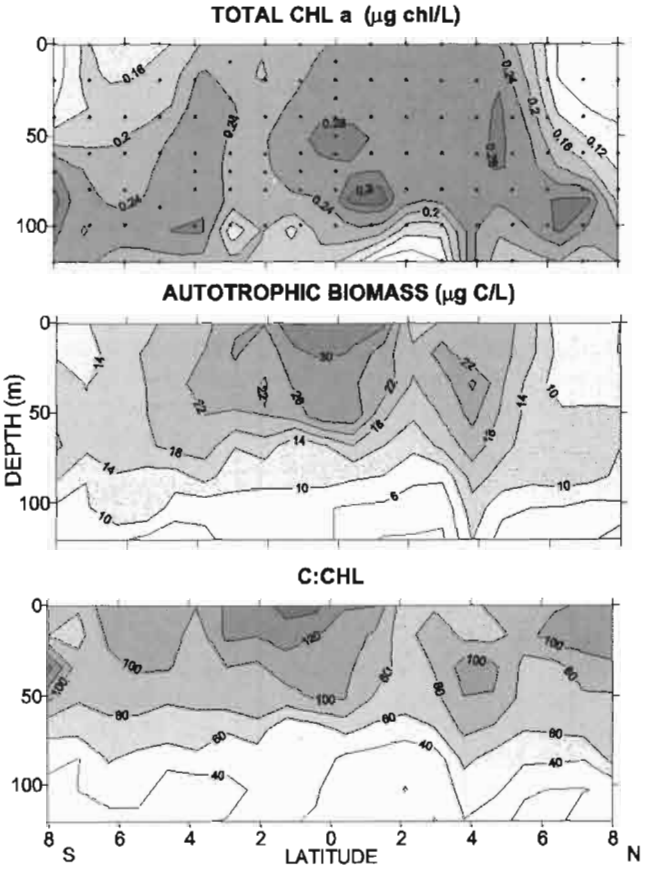

Figure 2. Depth distributions of total chlorophyll *a* (μg chl L^{-1}), auotrophic biomass (μg C L^{-1}), and C:chl ratios across the equatorial transect at 180°. Top panel shows the sampling points for all contoured figures.

3.2. Distributions and Biomass of Autotrophic Populations

[19] The total concentration of chlorophyll *a* (Tchl *a*), which represents all phytoplankton groups, was greatest between the equator and 5°N, with slightly elevated concentrations at 4°S (Figure 2). Tchl *a* averaged 0.21 μg L^{-1} and did not exceed 0.36 μg L^{-1}. South of 4°S and north of 5°N, Tchl *a* was greater in the 60–100-m depth strata than in surface waters, reflecting the presence of modest subsurface maxima (Table 1). On either side of the equator between 4°S and 5°N, Tchl *a* was fairly uniform throughout the water column. The lowest concentrations were north of 5°N in the NECC.

[20] Autotrophic biomass was distributed more symmetrically around the equator than Tchl *a*, with highest levels between 2°S and 2°N (Figure 2). Biomass averaged 15.4 μg C L^{-1} across the transect, ranging from as low as 1.2 μg C L^{-1} to a maximum of 32.3 μg C L^{-1} at the equator (Figure 2). With the exception of the NECC (6°–8°N), phytoplankton biomass was higher in the upper 50 m (mean = 20.0 μg C L^{-1}) than in the lower depth strata (mean = 13.0 μg C L^{-1}) (Table 1). Carbon to chlorophyll ratios varied with highest values (>120) in the surface waters

Table 1. Average Pigment Concentrations Over Two Depth Strata Along 180°[a]

Station	Depth	chl *a*	dv-chl *a*	Tchl *a*	chl *b*	dv-chl *b*	chl *c*	PE
8°S	0–50	0.05	0.06	0.10	0.01	n/a	0.01	0.10
	60–100	0.12	0.15	0.27	0.08	0.01	0.03	0.23
7°S	0–50	0.09	0.08	0.17	0.03	n/a	0.02	0.12
	60–100	0.12	0.11	0.23	0.06	n/a	0.03	0.11
6°S	0–50	0.09	0.07	0.16	0.04	n/a	0.02	0.10
	60–100	0.12	0.11	0.23	0.07	n/a	0.03	0.09
5°S	0–50	0.09	0.07	0.16	0.05	n/a	0.02	0.10
	60–100	0.14	0.11	0.25	0.08	0.02	0.03	0.08
4°S	0–50	0.14	0.12	0.25	0.06	n/a	0.02	0.11
	60–100	0.16	0.13	0.29	0.09	0.04	0.04	0.17
3°S	0–50	0.13	0.10	0.23	0.07	n/a	0.03	0.10
	60–100	0.12	0.09	0.21	0.08	0.05	0.03	0.09
2°S	0–50	0.12	0.08	0.21	0.06	n/a	0.03	0.07
	60–100	0.14	0.09	0.22	0.08	0.08	0.03	0.08
1°S	0–50	0.13	0.11	0.24	0.06	n/a	0.03	0.11
	60–100	0.15	0.09	0.23	0.08	0.03	0.03	0.07
0°	0–50	0.15	0.13	0.28	0.07	n/a	0.04	0.10
	60–100	0.16	0.11	0.27	0.07	0.02	0.04	0.07
1°N	0–50	0.14	0.12	0.26	0.06	n/a	0.03	0.09
	60–100	0.17	0.11	0.28	0.09	0.05	0.04	0.02
2°N	0–50	0.15	0.12	0.26	0.07	n/a	0.03	0.06
	60–100	0.13	0.09	0.22	0.07	0.04	0.03	0.02
3°N	0–50	0.13	0.11	0.24	0.07	n/a	0.03	0.10
	60–100	0.12	0.10	0.22	0.07	0.05	0.03	0.06
4°N	0–50	0.12	0.13	0.25	0.06	n/a	0.03	0.12
	60–100	0.12	0.13	0.25	0.06	0.01	0.03	0.11
5°N	0–50	0.15	0.13	0.28	0.06	n/a	0.03	0.11
	60–100	0.15	0.12	0.27	0.08	n/a	0.04	0.12
6°N	0–50	0.03	0.05	0.08	0.01	n/a	0.01	0.01
	60–100	0.11	0.14	0.25	0.06	0.06	0.03	0.04
7°N	0–50	0.03	0.04	0.07	0.01	n/a	0.01	0.01
	60–100	0.11	0.12	0.23	0.06	0.05	0.03	0.03
8°N	0–50	0.02	0.03	0.06	0.01	n/a	0.01	0.01
	60–100	0.06	0.08	0.14	0.03	0.06	0.02	0.03

[a]Monovinyl chlorophyll *a* (chl *a*), divinyl chlorophyll *a* (dv-chl *a*), total chlorophyll *a* (Tchl *a*), chlorophyll *b* (chl *b*), divinyl chlorophyll *b* (dv-chl *b*), chlorophyll *c* (chl *c*), and phycoerythrin (PE) concentrations are in μg L^{-1}.

from 3°S to 1°N (Figure 2). Near-surface ratios were lowest in the region from 2°N to 5°N. C:chl ratios in the 0–50-m depth range varied from 65 to 165 (mean = 100), while those from 60 to 100 m ranged from 33 to 93 with a mean of 56.

[21] Our FCM estimates of the abundance of *Prochlorococcus* spp. (PRO) and *Synechococcus* spp. (SYN) did not differ significantly from concurrent live measurements by shipboard FCM (J. Blanchot, personal communication). Live shipboard measurements were 96% and 92% of preserved sample estimates of PRO and SYN, respectively, based on Model II first principal component regression analysis (Live PRO = 10,000 + 0.96*(Preserved PRO), R = 0.94; Live SYN = 438 + 0.92*(Preserved SYN), R = 0.95). The close agreement between these independent analyses with different machines, operators and handling techniques supports the general accuracy of these population estimates.

[22] PRO abundance averaged 167,000 cells mL^{-1} in the upper 50 m and 105,000 cells mL^{-1} at depth, ranging over two orders of magnitude from 3,500 to 307,000 cells mL^{-1} (Table 2). In general, PRO were most abundant in the surface waters between 4°S and 2°N with a maximum at 3°S (Figure 3). PRO biomass ranged from 0.1 to 9.8 μg C L^{-1}, averaging 5.3 μg C L^{-1} in the upper 50 m. On average, PRO represented 28% of total autotrophic biomass, but station estimates were as high as 67% in the most oligotrophic waters of the NECC. The distribution of divinyl chlorophyll *a* (dv-chl *a*), the marker pigment for *Prochlorococcus* spp. differed markedly from PRO cell abundance, with higher concentrations deeper in the water column (maximum = 0.17 μg L^{-1}) and elevated pigment concentrations both south and north of the region of enhanced abundance (Figure 3).

[23] The presence of monovinyl chlorophyll *b* (chl *b*) can be attributed to different groups of phytoplankton, and its main source in this study was not always clear [*Neveux et al.*, 2003]. However, *Landry et al.* [2003] assumed that it was associated primarily with *Prochlorococcus* spp. on the basis of both negligible concentrations of other typical chl *b* containing groups and prior results from equatorial waters [*Bidigare and Ondrusek*, 1996; *Landry et al.*, 2000b]. Accordingly, the distribution of chl *b* bore some similarity to that of dv-chl *a* (Figure 3). Divinyl chlorophyll *b* (dv-chl *b*), characteristic of some PRO populations, was detectable only at depth (Table 1) with maxima generally located below 100 m. Concentrations were always <0.2 μg L^{-1} with the maximum at 6°N (data not shown). While a general feature in tropical and subtropical waters [*Mackey et al.*, 2002], the dv-chl *b* maximum at 4°N was much weaker than usual (<0.02 μg L^{-1}), presumably because of the effects of convergence and mixing.

[24] *Synechococcus* spp. (SYN) cells were most abundant at 3°S (maximum = 24,000 cells mL^{-1}), with a somewhat uniform concentration (15,000–18,000 cells mL^{-1}) in the surface waters between 2°N and 8°S (Figure 4 and Table 2). Across the transect, SYN were twice as abundant in the upper 50 m, averaging 12,700 cell mL^{-1} versus 6,800 cell mL^{-1} at depth. Although larger than PRO, SYN accounted for much less biomass, reaching only 2.7 μg C L^{-1} and averaging 1.3 μg C L^{-1} in the surface waters and 0.7 μg C L^{-1} from 60 to 100 m (Table 2 and Figure 4). Cell abundance throughout the water column dropped off dramatically north of 5°N as the transect crossed the NECC.

[25] The distribution of phycoerythrin (PE), the marker pigment for *Synechococcus* spp., conformed relatively closely to that of cell abundance, except that the highest pigment concentrations were found lower in the water column, a result of increasing PE per cell with decreasing light levels. Both FCM estimates of cell abundance and phycoerythrin concentrations showed areas of enhancement from 3°–4°S (30,000 cells mL^{-1} and 0.17 μg L^{-1}) and at 4°N (26,000 cells mL^{-1} and 0.14 μg L^{-1}). South of the equator, phycoerythrin concentrations exceeded 0.1 μg L^{-1} throughout much of the water column (Figure 4 and Table 1).

[26] The smaller photosynthetic eukaryotes (≤8-μm PEUKS) were most concentrated at the equator reaching 8,500 cells mL^{-1}, and decreased in abundance to the north and south (Figure 5 and Table 2). The larger size fraction (> 8 μm) was more abundant in the upper 50 m from 2°S to 4°N, with a maximum of 77 cells mL^{-1} at 3°N (Figure 5). Both size fractions were modestly enhanced at 4°N. The biomass of the small phytoplankton was concentrated symmetrically in three locations, 4°S, 0°, and 4°N (Figure 5). Biomass ranged from 0.7 μg C L^{-1} to 17.4 μg C L^{-1}, averaging 8.0 μg C L^{-1} in the upper 50 m and 5.0 μg C L^{-1} at depth (Table 2). It should be noted that spatial trends in the biomass of the smaller PEUKS reflected trends in cell

Table 2. Average Abundance and Biomass of Autotrophic Microorganisms in Two Depth Strata Along 180°[a]

		Abundance, cell mL^{-1}				Biomass, μg C L^{-1}				
				PEUKS				PEUKS		
Station	Depth	PRO	SYN	≤8 μm	>8 μm	PRO	SYN	≤8 μm	>8 μm	AC
8°S	0–50	167,000	14,900	2,100	30	5.4	1.5	3.2	6.1	17.7
	60–100	172,000	10,800	2,600	40	5.5	1.1	4.0	4.8	15.4
7°S	0–50	151,000	15,300	2,200	20	4.8	1.5	3.9	2.7	13.0
	60–100	102,000	7,500	2,000	20	3.3	0.8	3.6	2.6	10.3
6°S	0–50	117,000	19,000	2,500	40	3.7	1.9	5.7	5.4	16.8
	60–100	103,000	14,300	2,100	40	3.3	1.5	4.8	6.5	16.0
5°S	0–50	130,000	15,300	4,200	30	4.2	1.6	10.3	2.8	19.1
	60–100	91,000	7,800	2,600	20	2.9	0.8	6.2	4.0	13.9
4°S	0–50	167,000	17,800	5,700	30	5.4	1.8	11.3	4.2	22.7
	60–100	103,000	9,900	3,900	40	3.3	1.0	7.7	5.1	17.1
3°S	0–50	283,000	22,300	5,800	30	9.0	2.2	9.8	4.0	24.9
	60–100	156,000	14,200	2,200	30	5.8	1.6	3.3	3.4	14.4
2°S	0–50	202,000	15,100	6,600	50	6.5	1.5	8.5	6.8	23.3
	60–100	122,000	9,300	4,900	30	3.9	1.0	6.3	3.8	14.9
1°S	0–50	222,000	15,600	5,700	50	7.1	1.6	11.3	10.7	30.7
	60–100	78,000	4,700	3,600	30	2.5	0.5	7.3	2.8	13.0
0°	0–50	220,000	13,900	8,200	50	7.0	1.4	16.0	5.1	29.5
	60–100	117,000	7,400	6,000	30	4.5	0.9	8.7	3.2	23.1
1°N	0–50	222,000	15,700	6,200	60	7.1	1.6	10.7	8.1	27.5
	60–100	70,000	2,900	2,900	30	2.2	0.3	5.1	3.3	10.9
2°N	0–50	115,000	7,500	3,400	50	3.7	0.8	6.8	5.9	17.1
	60–100	47,000	1,500	2,000	10	1.5	0.2	4.1	1.1	6.9
3°N	0–50	112,000	12,500	3,100	60	3.6	1.2	7.6	8.3	20.7
	60–100	49,000	3,700	1,500	30	1.6	0.4	3.7	3.4	9.0
4°N	0–50	140,000	15,600	5,200	50	4.5	1.6	11.5	4.5	22.1
	60–100	126,000	9,500	3,800	40	4.1	1.0	8.2	6.4	19.6
5°N	0–50	134,000	11,500	4,100	60	4.3	1.1	8.5	4.7	18.5
	60–100	73,000	5,700	2,300	50	2.3	0.6	4.9	1.3	9.0
6°N	0–50	132,000	1,000	600	10	4.2	0.1	1.1	2.0	7.4
	60–100	107,000	2,100	1,600	20	3.4	0.2	3.0	3.4	10.0
7°N	0–50	157,000	700	500	10	5.0	0.1	0.8	1.6	7.4
	60–100	117,000	1,400	1,800	20	3.7	0.1	3.1	1.9	8.9
8°N	0–50	129,000	400	600	10	4.1	0.0	1.2	0.9	5.9
	60–100	133,100	700	1,000	30	4.2	0.1	2.1	2.3	8.8

[a]PRO and SYN refer to *Prochlorococcus* spp. and *Synechococcus* spp., respectively. Photosynthetic eukaryotes (PEUKS) are separated into two size classes, ≤8 μm and >8 μm. AC is total autotrophic biomass.

abundance, such that latitudinal differences were not an artifact of chosen carbon per cell conversion factors. Biomass of the larger PEUKS was similar in magnitude, averaging 5.0 μg C L^{-1} in the upper layer and reaching a maximum of 14.3 μg C L^{-1}. Despite the skew in their abundance distributions to the north, the highest biomass of >8-μm PEUKS was more or less symmetrical in equatorial surface waters between 2°S and 3°N (Figure 5 and Table 2).

[27] Diatoms were never a significant component of the total phytoplankton biomass and were often too scarce to be counted with high precision; in such instances, biomass was negligible. Diatom carbon reached a maximum of 4.0 μg C L^{-1} at the surface at 1°S and averaged only 0.2 μg C L^{-1} across the study region (Figure 6). In general, diatom carbon comprised 2% of phytoplankton. Photosynthetic dinoflagellates, on the other hand, were the most abundant large phytoplankton across the transect (14% of autotrophic carbon), averaging 2.3 μg C L^{-1} and reaching up to 10 μg C L^{-1} in the surface at 1°N (Figure 6). Chlorophyll *c* (chl *c*), a pigment common to various groups of eukaryotes, was more broadly distributed with latitude than either diatoms or dinoflagellates, and conformed closely to the pattern for total chl *a* (Figure 6). Although other phytoplankton groups were not distinguished taxonomically in our samples, we assume that chl *c* along 180° was largely associated with pyrmnesiophytes and pelagophytes on the basis of high pressure liquid chromatography (HPLC) analyses of group-specific accessory pigments at 0° and 3°S [*Landry et al.*, 2003].

3.3. Distributions and Biomass of Heterotrophic Populations

[28] Heterotrophic biomass, including protistan grazers and heterotrophic bacteria (HBACT), exceeded 25 μg C L^{-1} in surface maxima at 6°S, 2°N, and 5°N (Figure 7). An additional area of high biomass (33 μg C L^{-1}) was located at 60 m at 3°N. For the transect as a whole, total heterotrophic carbon (HC) almost equaled phytoplankton biomass, averaging 13 μg C L^{-1} and ranging from 5 to 36 μg C L^{-1}. HC was higher in the upper 50 m, averaging 16 μg C L^{-1} versus 11.5 μg C L^{-1} at depth (Table 3). North of 5°N, heterotrophic biomass did, in fact, exceed autotrophic biomass throughout the water column (Tables 2 and 3).

[29] HBACT carbon (BC), corresponding to bacterial cell numbers, showed a distribution similar to that of PRO, with the highest abundances at 3°S and enhanced concentrations between 6°S and 2°N (Figure 8 and Table 3). At 3°S, densities reached 1.1 × 10^6 cell mL^{-1}, corresponding to 12.4 μg C L^{-1}. Integrated to 100-m depth, cell numbers and

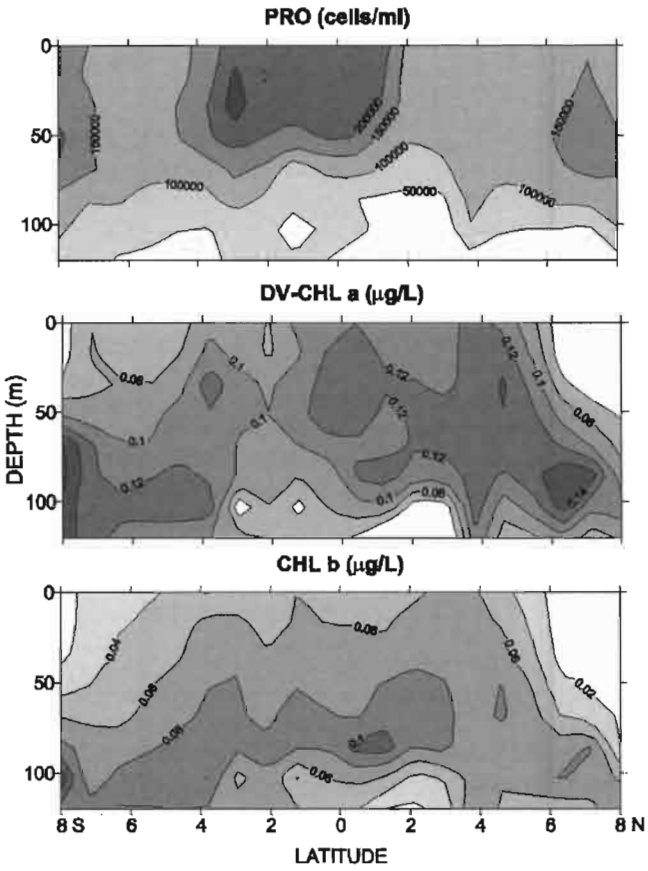

Figure 3. Depth distributions of *Prochlorococcus* spp. (PRO cells mL^{-1}), divinyl chlorophyll *a* (dv-chl *a*), and chlorophyll *b* in µg L^{-1} across the equatorial transect at 180°.

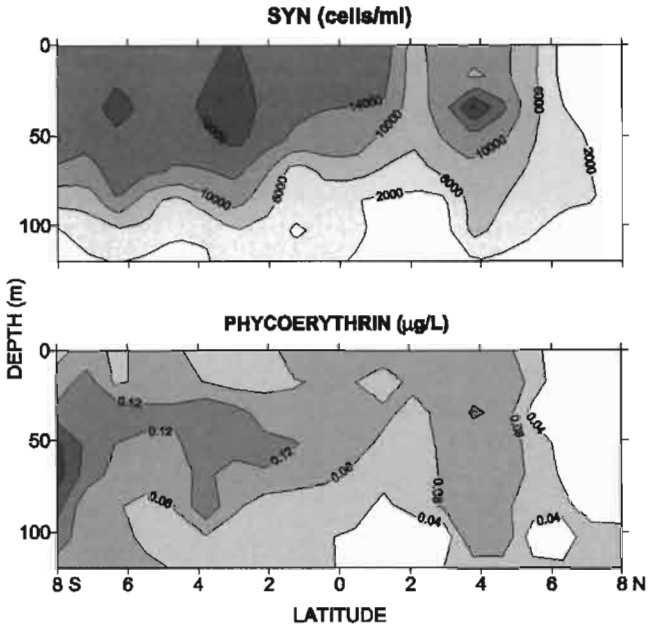

Figure 4. Depth distributions of *Synechococcus* spp. (SYN cells mL^{-1}) and the pigment phycoerythrin (PE) in µg L^{-1} across the equatorial transect at 180°.

biomass averaged 5.9×10^5 cells mL^{-1} and 6.5 µg C L^{-1}, respectively. BC was only slightly higher in the upper 50 m than from 60 to 100 m (Table 3). Differences in the 90° light scattering properties of bacterial cells, a common proxy for cell size [*Binder et al.*, 1996; *Brown and Landry*, 2001], were apparent but did not show a strong relationship to abundance (Figure 8). Slightly larger cells were found at the surface between the equator and 2°N, as well as north of 5°N in the NECC, but there was no obvious difference in cell sizes at 3°S, the site of maximum abundance. Also notable was an area from 4° to 5°N where smaller cells extending throughout the water column.

[30] The abundance and biomass of ≤8-µm grazers showed patchy, but similar distributions (Figure 9). Abundances ranged from 100 to 2,000 cells mL^{-1} and averaged 600 cells mL^{-1} (Table 3). Biomass averaged 1.6 µg C L^{-1}, with a maximum of 4 µg C L^{-1}. Abundance and biomass in the upper 50 m were only slightly higher than at depth: 700 cells mL^{-1} and 1.8 µg C L^{-1} versus 500 cells mL^{-1} and 1.5 µg C L^{-1}, respectively. Small grazer biomass was concentrated between the equator and 2°N and at the surface from 3° to 5°N (Figure 9).

[31] The distribution of >8-µm grazers was slightly more uniform, ranging from 6 to 50 cells mL^{-1} and averaging 22 cells mL^{-1}. Their biomass exceeded that of the ≤8-µm grazers, averaging 5 µg C L^{-1} with a maximum of 26 µg

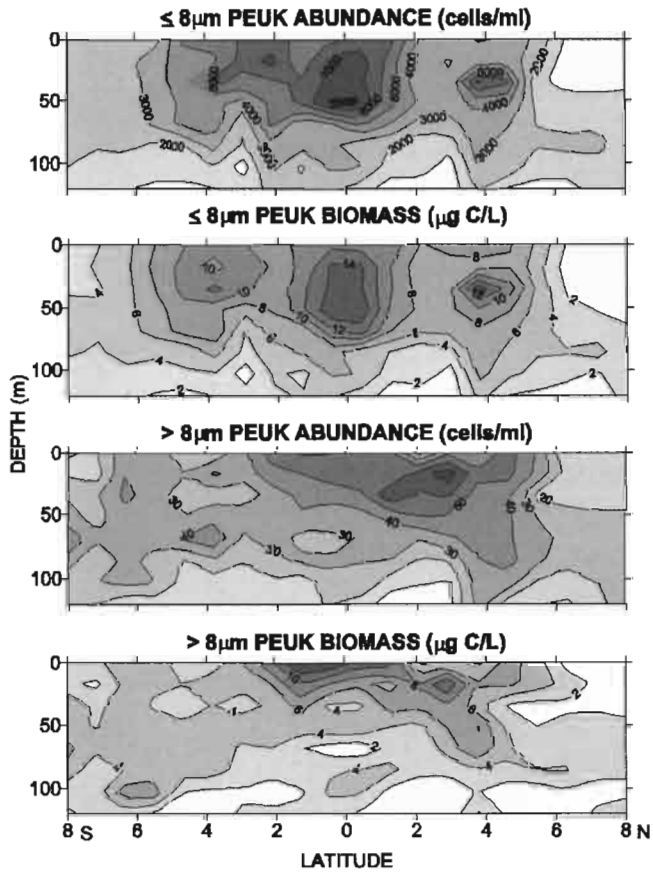

Figure 5. Depth distributions of ≤8-µm and >8-µm eukaryotic phytoplankton across the equatorial transect at 180°.

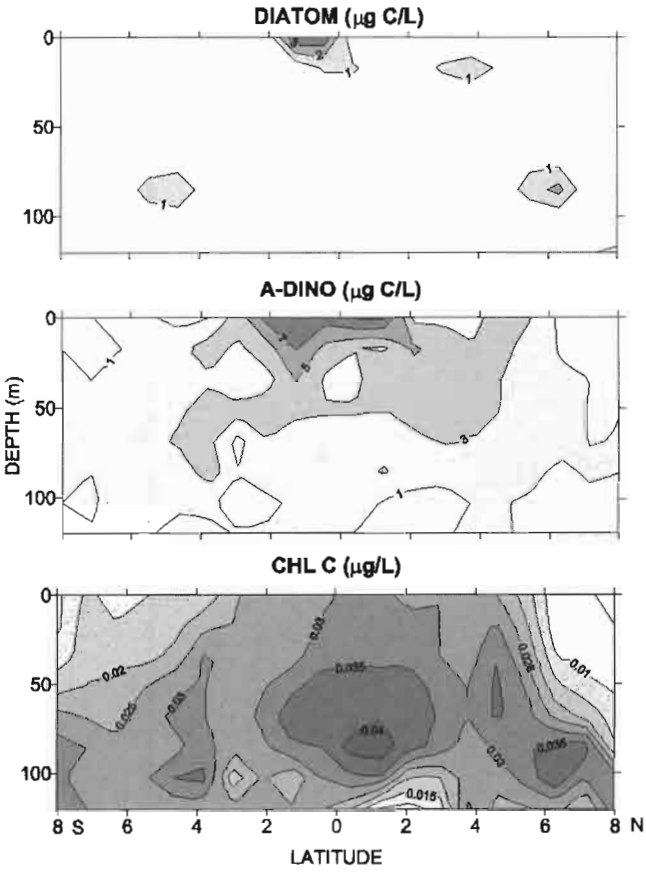

Figure 6. Depth distributions of autotrophic carbon (µg C L^{-1}) attributable to >8-µm diatoms and >8-µm autotrophic dinoflagellates (a-dino) and chlorophyll *c* (µg chl L^{-1}) across the equatorial transect at 180°.

C L^{-1}. Both the abundance and biomass of the larger heterotrophic protists were higher in the upper 50 m than from 60 to 100 m (Table 3). High biomass of >8-µm grazers was found between the equator and 2°N, as well as coincident with a modest concentration of small grazers at 5°N (Figure 9). Biomass of larger grazers also exceeded 20 µg C L^{-1} at 3°N at 60 m. Nearly all of the larger protistan grazers were dinoflagellates. Given the widespread mixotrophic habits of this protistan group [*Porter*, 1988; *Sanders and Porter*, 1988; *Bockstahler and Coats*, 1993; *Li et al.*, 1996], the biomass of potential grazers was likely underestimated by counting all autofluorescent dinoflagellates as "autotrophs."

3.4. Depth-Integrated Biomass

[32] Integrated biomass (0 to 100 m) of the three prokaryote groups showed the same latitudinal trends, with higher biomass south of the equator decreasing modestly to the north (Figure 10 and Table 4). Of the three groups, HBACT had the highest integrated biomass, followed by PRO and SYN. Each group exhibited enhanced biomass at 3°S, 0°, and 4°N (Figure 10). Integrated biomass of ≤8-µm PEUKS clearly increased from 8°S to a maximum at the equator, dropping off sharply north of the equator and exhibiting peaks at both 4°S and 4°N. Integrated biomass of the >8-µm PEUKS was fairly constant from 8°S to 5°N and decreased north of 5°N (Figure 10 and Table 4). Compared to bacteria and eukaryotic phytoplankton, the biomass of protistan grazers followed an increasing trend from south to north, with the larger grazers showing a stronger trend and a peak at 5°N. The ≤8-µm grazers exhibited a slight maximum at 4°N. Both integrated autotrophic carbon (AC) and total carbon (TC) increased from 8°S to a peak at the equator and decreased north of the equator (Figure 10 and Table 4). Overall, there is a slight south to north trend in TC and AC because of low biomass in the NECC north of 5°N. Integrated heterotrophic carbon (HC), including both HBACT and protistan grazers, was fairly constant across the transect, with a slight increase to the north.

[33] For the 100-m water column, biomass-weighted mean carbon to chlorophyll ratios were highest (mean = 103) in the region from 3°S to 1°N, with the exception of a high value (114) at 8°S (Table 5). Prokaryotic organisms generally comprised less than 50% of the total integrated biomass, exceeding that only slightly at 3°S (54%; Table 5). Between 1°S and 5°N, the prokaryote contribution to total community biomass was particularly low (<40%). There was no apparent difference between the contribution of prokaryotes in the upper 50 m and from 60 to 100 m (data not shown).

[34] Integrated living microbial biomass represented 44 to 88% of combusted particulate organic carbon (POC) (Y. Suzuki, unpublished data, and Table 5). The greatest contribution of microbial biomass appeared to be in the vicinity of the equator (2°S–1°N), but the lack of POC data at 3°S and the equator makes it difficult to discern a clear pattern. Autotrophic carbon (AC) exceeded heterotrophic carbon (HC) from 8°S to 1°N (AC:HC > 1; Table 5). North of 1°N, heterotrophic biomass equaled or exceeded autotrophic biomass (AC:HC < 1) with the exception of 4°N (AC:HC = 1.5). The ratio of biomass between the two trophic modes was similar in the upper 50 m and in the lower depth strata (mean = 1.1 for both).

4. Discussion

[35] To our knowledge, the present study marks the most comprehensive assessment of microbial community structure (biota < 200 µm) in the central equatorial Pacific. Given the relatively recent discovery of *Prochlorococcus* spp. [*Chisholm et al.*, 1988, 1992] and the development of flow cytometric methods [*Olson et al.*, 1990a, 1990b; *Monger*

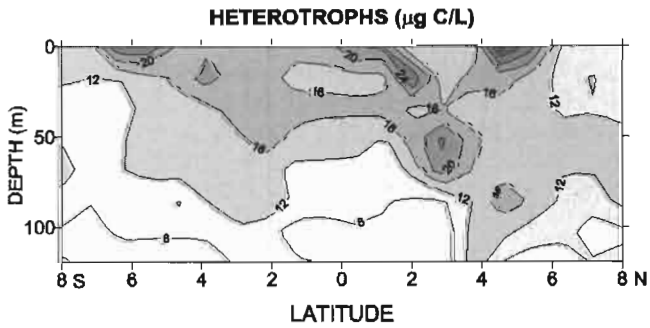

Figure 7. Depth distributions of total heterotrophic carbon (µg C L^{-1}) across the equatorial transect at 180°.

Table 3. Average Abundance and Biomass of Heterotrophic Bacteria and Protists in Two Depth Strata Along 180°[a]

		Abundance, cells mL^{-1}			Biomass, $\mu g\ C\ L^{-1}$			
Station	Depth	HBACT	≤8 μm	>8 μm	HBACT	≤8 μm	>8 μm	HC
8°S	0–50	614,000	100	20	6.8	0.6	0.4	8.1
	60–100	578,000	330	10	6.4	1.3	3.4	11.0
7°S	0–50	609,000	210	10	6.7	1.0	3.9	11.6
	60–100	517,000	180	10	5.7	0.5	1.4	7.6
6°S	0–50	756,000	510	20	8.3	0.9	7.6	16.8
	60–100	650,000	460	20	7.1	1.3	3.5	11.9
5°S	0–50	757,000	650	20	8.3	0.8	4.1	15.3
	60–100	569,000	220	10	6.3	0.6	3.8	10.7
4°S	0–50	826,000	500	30	9.1	1.3	8.1	18.4
	60–100	745,000	530	20	8.2	1.5	2.5	12.1
3°S	0–50	1,009,000	810	30	11.1	1.9	3.9	17.2
	60–100	927,000	590	10	10.2	1.3	2.4	13.5
2°S	0–50	904,000	590	30	9.9	1.5	6.6	18.0
	60–100	776,000	400	20	8.5	0.9	5.3	14.8
1°S	0–50	850,000	420	30	9.4	0.9	6.2	16.4
	60–100	480,000	290	20	5.3	1.0	3.0	9.3
0°	0–50	894,000	1280	22	9.8	2.4	4.9	16.6
	60–100	839,000	710	23	9.5	1.5	6.4	14.9
1°N	0–50	655,000	1540	30	7.2	3.1	8.6	18.8
	60–100	363,000	630	14	4.0	1.3	2.5	7.8
2°N	0–50	510,000	1060	30	5.6	2.4	10.1	18.1
	60–100	332,000	650	10	3.6	1.9	1.0	6.5
3°N	0–50	610,000	650	30	6.7	2.0	6.4	15.1
	60–100	386,000	710	10	4.2	2.3	8.8	15.3
4°N	0–50	589,000	920	30	6.5	3.1	5.3	14.8
	60–100	586,000	750	30	6.5	2.6	4.4	13.4
5°N	0–50	611,000	810	40	6.7	2.4	17.0	26.9
	60–100	579,000	570	20	6.4	1.9	11.4	21.0
6°N	0–50	351,000	650	30	3.9	1.6	5.6	11.0
	60–100	340,000	690	20	3.7	2.3	4.9	10.9
7°N	0–50	327,000	630	20	3.6	1.6	5.5	10.6
	60–100	348,000	530	10	3.8	1.8	4.0	9.6
8°N	0–50	310,000	460	30	3.4	1.7	4.1	9.3
	60–100	354,000	520	20	3.9	1.2	8.2	13.6

[a]HBACT, ≤8 μm and >8 μm refer to heterotrophic bacteria; ≤8-μm heterotrophic protists and >8-μm heterotrophic protests, respectively. HC is heterotrophic carbon.

and Landry, 1993], it was not possible to account for the smallest primary producers in early studies. Since this advance, there has also been a tendency for specialists to focus on specific components of the microbial community such as the microphytoplankton [*Kaczmarska and Fryxell*, 1995; *Iriarte and Fryxell*, 1995], picoplankton [*Binder et al.*, 1996; *Landry et al.*, 1996; *Blanchot and Rodier*, 1996], or heterotrophic nanoplankton [*Vors et al.*, 1995] rather than the community as a whole. The two studies that have attempted a broader assessment [*Chavez et al.*, 1996; *Ishizaka et al.*, 1997] have inferred PRO biomass from divinyl chlorophyll *a* concentrations. As evident from the very different distributions of PRO cells and dv-chl *a* in Figure 3, the use of pigments as a PRO biomass proxy is problematic, whether because of photoacclimation or genetic differences.

[36] Because the alkaline Lugol's slide protocol was developed with the intention of allowing quantitative experimental studies with delicate ciliates [*Sherr and Sherr*, 1993], we assumed that it would be adequate for ciliate biomass assessment in the present study. Subsequently, we have found it to be substantially less suitable for that purpose than the more traditional inverted microscopical enumeration of acid Lugol's preserved samples. As a consequence, our estimates of total "grazer" biomass did

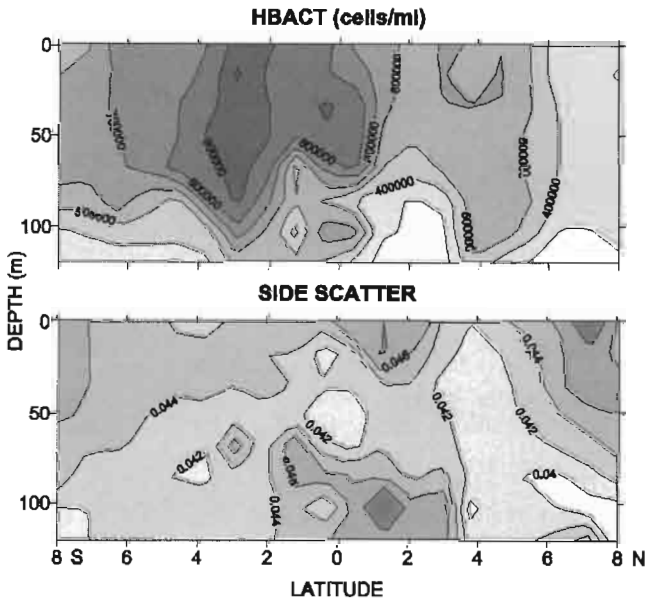

Figure 8. Abundance (cells mL^{-1}) and cellular side scatter of heterotrophic bacteria across the equatorial transect at 180°. Mean side scatter per cell (in arbitrary units) is a proxy for cell size.

not include ciliated protozoa. Previous estimates of ciliate biomass in equatorial waters have ranged from negligible ($< 0.1–0.2$ μg C L^{-1}) in the central region at 140°W [*Verity et al.*, 1996; *Stoecker et al.*, 1996] to 2 μg C L^{-1} further east at 105°W [*Landry et al.*, 2000b]. Taking into consideration the dominance of heterotrophic dinoflagellates in the western equatorial Pacific [*Ishizaka et al.*, 1997], it has been suggested that ciliates might increase in relative importance with system richness from west to east [*Landry and Kirchman*, 2002]. In our study, the relatively large biomass of >8-μm heterotrophic dinoflagellates would be consistent with the diminished importance of ciliates, as was the latitudinal distribution of ciliates reported by *Chavez et al.* [1996] during non-El Niño conditions. For these reasons, we expect that ciliates typically represent a small component of the protistan grazer community in the present study region.

4.1. Community Composition and Structure

[37] At a very general level, the composition of the equatorial microbial community is known [*Le Bouteiller et al.*, 1992; *Mackey et al.*, 2002; *Landry and Kirchman*, 2002]. The phytoplankton community is characterized by relatively constant low levels of biomass, the dominance of small species and a paucity of large bloom-forming diatoms. Less well understood is the inherent variability in community composition, the interplay of autotrophic and heterotrophic populations and the community responses to varying physical forces.

[38] Although the otherwise detailed community study of *Chavez et al.* [1996] did not account for PRO and HBACT, it provides an appropriate basis of comparison for eukaryotic populations. The only significant difference in carbon conversion factors was our use of FCM estimates of small eukaryotic phytoplankton (utilizing latitudinal-specific microscopically derived conversion factors for cells within the 1.5–8-μm size range), whereas *Chavez et al.* [1996] applied a constant cellular carbon factor for eukaryotic picoplankton (<2 μm) and a biovolume-dependent carbon conversion factor for eukaryotes >2 μm. Despite this difference, our biomass estimates were in generally good agreement. *Chavez et al.* [1996] reported that the surface standing stock of phytoplankton in the equatorial region fell within the fairly narrow range of 15–25 μg C L^{-1}. For the EBENE transect, average phytoplankton biomass (0–50 m) in the SEC ranged from 17–30 μg C L^{-1}. Likewise, *Chavez et al.* [1996] reported average phytoplankton and grazer biomass of 20 and 5 μg C L^{-1}, respectively, versus our averages of 17 and 7 μg C L^{-1}.

[39] The picoplankton of the tropical Pacific have been described as the background over which the dynamics of the larger organisms are imprinted [*Landry and Kirchman*, 2002]. Accordingly, the integrated biomass of PRO, SYN, and HBACT each varied by only a factor of 2 or less throughout the equatorial region from 5°S to 5°N (Table 4 and Figure 10). The relative constancy of these populations reinforces the concept of a strong and stable microbial food web in the equatorial Pacific, which is presumed to derive from a close coupling of growth, grazing and remineralization processes [*Landry et al.*, 1997; *Landry et al.*, 2000a, 2000b; *Landry and Kirchman*, 2002]. Although the total population of the picoplankton may be somewhat predictable, the distributions are not. During both El Niño conditions and a normal upwelling, *Landry et al.* [1996] reported a PRO abundance minimum between 2°S and 2°N, and a SYN minimum at 0° during El Niño. However, the distribution of PEUKS was similar to that in the present study with areas of accumulation at the equator and on each side. These differences in PRO and SYN distributions raise the question of what is "typical" across the equator and more importantly, why and how do they vary?

[40] The variability in autotrophic carbon during EBENE was attributed mostly to the ≤8-μm cells that dominated phytoplankton biomass, with the exception of the anomalous community at 3°S. Within this size class, true "picoeukaryotes" (<2-μm) were negligible, and the larger flagellates (often dinoflagellates) were biomass dominants. *Chavez et al.* [1996] also reported the dominance of 5–20 μm dinoflagellates and noted that while the magnitude of autotrophic carbon changed between El Niño and non-El Niño conditions, the relative proportions of each group did not. If the relative proportions of functional groups are, in fact, constant over changing conditions in the central equatorial Pacific, we would expect that the biomass of >8-μm autotrophs typically equal that of the picophytoplankton, while ≤8-μm phytoflagellates dominate the phytoplankton biomass.

[41] The integrated biomass of large protistan grazers exceeded that of small grazers at all stations. The biomass of ≤8-μm grazers was fairly constant, pointing to their ability to exploit the smaller, more consistently available picoplankton prey. Larger grazer biomass was more prevalent in the north and seemed to follow the distributions of both large and small phytoplankton, which is not surprising given their broader size range (8–200 μm) and thus feeding capabilities. Mesozooplankton grazers, primarily copepods, were distributed asymmetrically to the south, with the exception of 4°N [*Le Borgne et al.*, 2003]. The distributional differences among these components of the food web suggests some regulation by mesozooplankton grazing of larger phytoplankton and micrograzers in the southern transect, with possible cascading influences on lower trophic levels [*Calbet and Landry*, 1999].

[42] For samples from the upper 50 m, the relationship between HBACT and Tchl *a* was quite strong [$\log_{10}(\text{HBACT}) = 6.2 + 0.51 \log_{10}(\text{chl})$, $R = 0.76$]. This relationship is strikingly similar to the *Cole et al.* [1988] cross-ecosystem result: $\log_{10}(\text{HBACT}) = 6.0 + 0.53 \log_{10}(\text{chl})$, $R = 0.75$. *Cho and Azam* [1990] reported that the relationship between HBACT and chl *a* concentration was poor for oligotrophic chlorophyll concentrations <0.5 μg chl L^{-1}. In contrast, our relationship held over the narrow range of chlorophyll encountered, all of which where <0.5 μg chl L^{-1}, and was somewhat stronger (higher slope) than that reported by *Buck et al.* [1996] for the tropical North Atlantic.

[43] Across the EBENE transect, the relationship between HBACT carbon (BC) and autotrophic carbon (AC) was similar to that of abundance and chlorophyll: $\log_{10}(\text{BC}) = 0.015 + 0.65 \log_{10}(\text{AC})$, $R = 0.89$. In the divergence zone (2°S–2°N) however, the results were quite different: $\log_{10}(\text{HBACT}) = 5.5–0.58 \log_{10}(\text{chl})$, $R = 0.30$ versus $\log_{10}(\text{BC}) = 0.06 + 0.61 \log_{10}\text{AC}$, $R = 0.61$. Clearly, there was an uncoupling between phytoplankton carbon and

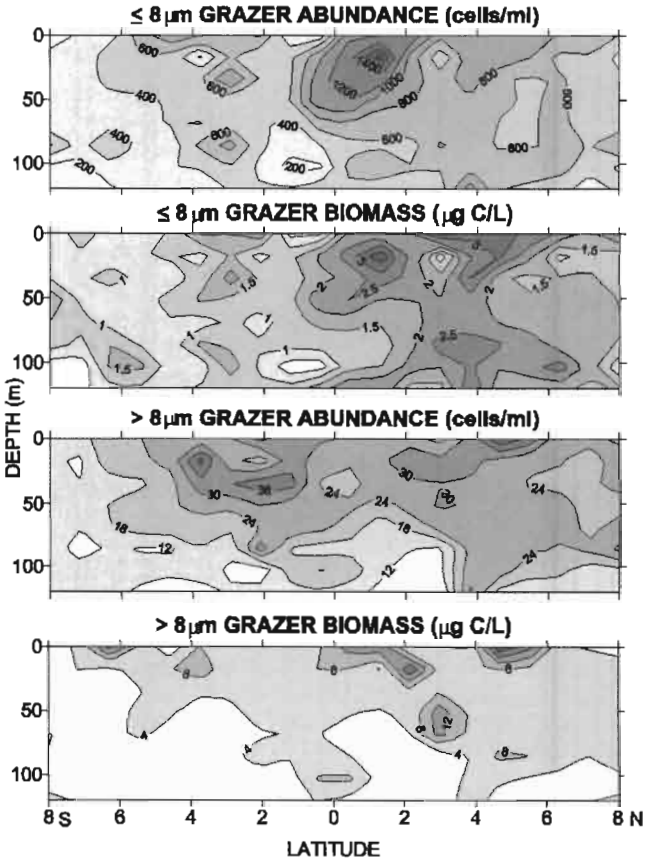

Figure 9. Depth distributions of ≤8-µm and >8-µm grazers across the equatorial transect at 180°.

chlorophyll in this divergence zone such that BC followed the biomass of the autotrophs and varied inversely with chlorophyll.

[44] In contrast to previous results from 140°W [*Iriarte and Fryxell*, 1995], diatoms were a minor component of the microphytoplankton. Our diatom abundance estimates (range = <1 – 20, mean = 3 cells mL^{-1}) were well within the ranges reported in nonblooming equatorial waters (2–77 cells mL^{-1} given by *Hasle* [1959]; 1–10 cell mL^{-1} given by *Semina* [1972]; ≤1 cells mL^{-1} given by *Kaczmarska and Fryxell* [1995]; and 1–5 cell mL^{-1} given by *Iriarte and Fryxell* [1995]). The slight enhancement of diatom biomass seen at the equator (Figure 6) is consistent with the maximum in both biogenic silica concentrations and production rates [*Leynaert et al.*, 2001]. Although negligible in biomass, the abundance of rare, "net" caught diatoms (i.e., >200 µm) was highest south of the equator with a maximum at 3°S [*Le Borgne et al.*, 2003], the station with maximum prokaryote biomass.

[45] Previous JGOFS studies, as well as the IronEx II project, revealed an equatorial diatom community dominated by small (<10 µm), rapidly growing pennate diatoms, some of which were grazed by microzooplankton and thus integrated into the microbial food web [*Latasa et al.*, 1997, *Landry et al.* 2000a, 2000b; *Landry et al.*, 2003]. Not only were small pennate diatoms noticeably scarce along 180°, the modest diatom biomass was comprised of large (>100 µm) cells such as *Thalassionema/Thalassiothrix* spp. and centric forms including *Chaetoceros* spp. and *Rhizosolenia* spp. Given the absence of iron data in our study, it is unknown whether that could have been a stimulatory factor for large cells. A second and not mutually exclusive possibility is that microzooplankton grazing constrained the population growth of smaller diatoms while the largest cells escaped predation. Despite the different composition of the diatom community in this study, diatom growth rates were as high (1.0–1.6 d^{-1}) as previously reported estimates (*Landry et al.* [2003] versus *Latasa et al.* [1997] and *Landry et al.* [2000a]). Given the large size of cells that dominated diatom biomass, they likely contributed disproportionately to export flux, as suggested by *Leynaert et al.* [2001] from biogenic silica studies.

[46] In both the nitrate-impoverished northern portion of the SEC and the picoplankton-dominated waters of the NECC, total heterotrophic biomass exceeded phytoplankton biomass. This "inverted structure" may be characteristic of oligotrophic waters [*Fuhrman et al.*, 1989; *Buck et al.*,

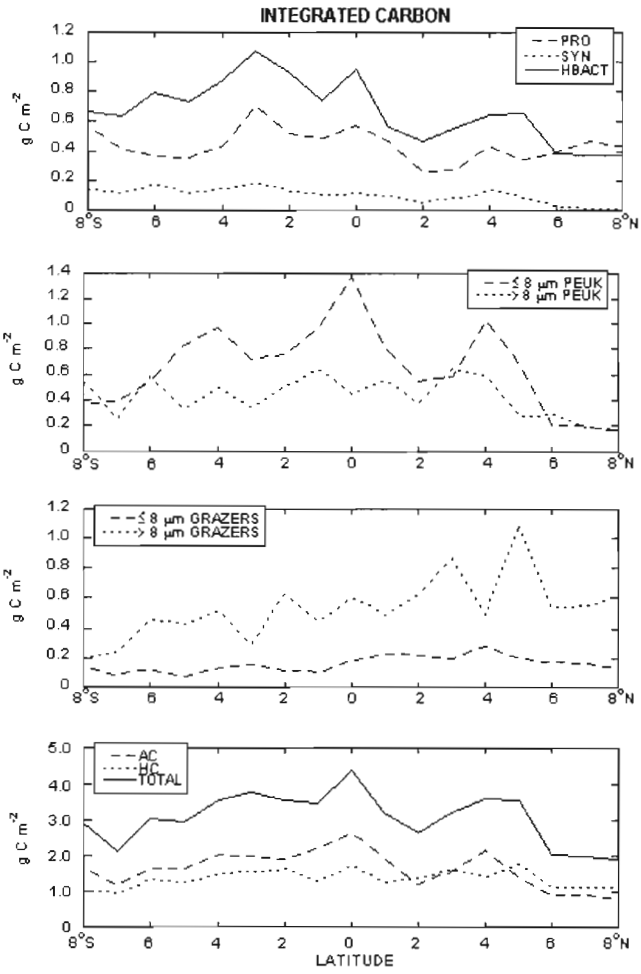

Figure 10. Latitudinal distribution of 0–100 m integrated carbon (g C m^{-2}) attributed to various components of the microbial community across the equatorial transect at 180°. PRO, *Prochlorococcus* spp.; SYN, *Synechococcus* spp.; HBACT, heterotrophic bacteria; PEUKS, photosynthetic eukaryotes; AC, autotrophic carbon; HC, heterotrophic carbon; and TOTAL, total microbial carbon.

Table 4. Integrated (0–100 m) Carbon Estimates (mg C m^{-2}) for Autotrophic, Heterotrophic, and Total Carbon Fractions[a]

		Autotrophs				Heterotrophs				
Station	PRO	SYN	≤8 μm	>8 μm	AC	HBACT	≤8 μm	>8 μm	HC	Total
8°S	560	130	360	550	1670	670	130	190	990	2920
7°S	410	120	380	250	1170	630	80	240	950	2120
6°S	360	180	540	580	1660	790	110	460	1360	3020
5°S	350	120	830	340	1640	730	70	430	1230	2940
4°S	440	140	970	500	2050	880	140	520	1530	3580
3°S	710	190	720	360	2000	1070	160	300	1550	3770
2°S	520	130	750	510	1910	930	110	620	1660	3570
1°S	490	100	950	650	2190	740	110	450	1300	3490
0°	580	120	1380	450	2660	950	190	600	1740	4410
1°N	470	100	820	560	1940	560	220	490	1270	3210
2°N	260	50	540	380	1230	470	210	620	1390	2650
3°N	270	80	580	640	1570	560	200	860	1620	3200
4°N	440	130	1030	590	2190	650	280	490	1420	3610
5°N	340	90	680	280	1390	660	210	1090	1780	3560
6°N	400	20	210	290	920	390	180	540	1110	2020
7°N	470	13	210	190	890	380	170	550	1120	2000
8°N	430	10	160	160	720	360	140	630	1130	1850

[a]Column designations are as in Tables 2 and 3.

1996], but comparison among studies is confounded by differences in the assessment of photosynthetic and heterotrophic bacteria and different cellular carbon conversion factors. For example, *Buck et al.* [1996] suggested that heterotrophy (HC > AC) had been largely overestimated, particularly in tropical regions of the North Atlantic. However, carbon conversion factors for PRO, SYN, and PEUK from the present study would reduce their autotrophic biomass by 30–50%, increasing the spatial extent of heterotrophic dominance substantially. In the present study region, HC > AC at chlorophyll concentrations <0.13 μg C L^{-1}. However, this must be interpreted with caution in light of the uncoupling between AC and Tchl *a* as noted above.

[47] We did not take into account possible depth, latitudinal, or diel variations in the size and cellular carbon content of autotrophic or heterotrophic bacteria. Increases in PRO, SYN, and HBACT cell size with depth have been documented in tropical Pacific Ocean and Arabian Sea waters [*Binder et al.*, 1996; *Shalapyonok et al.*, 2001] as have increases in PRO and SYN cell size in response to tropical instability waves and iron enrichment [*Binder et al.*, 1996; *Landry et al.*, 2000b]. Contrary to previous findings, we did not see clear indications of increases in PRO, SYN, or HBACT cell sizes with depth, based on FCM side scatter measurements.

[48] While only modestly represented in the contour of side scatter (Figure 8), the increase in the average side scatter per cell of HBACT from 0° to 2°N represents the presence of a substantial and distinct population of large bacteria as seen in flow cytometric scattergrams (side scatter versus blue fluorescence, data not shown). *Binder et al.* [1996] reported a similar distinct population of large abundant bacteria whose appearance was not correlated with any environmental parameters. It is difficult to tell whether the presence of large bacteria in our study was a feature of the returning, and thus older, southward branch of the TIW or whether it was a more random shift as suggested by *Binder et al.* [1996]. Presumably size would be responsive to the amount or type of DOM available or to changes in the intensity as well as size structure of bacterivorous grazers.

4.2. Physical and Biological Relationships

[49] Previous JGOFS equatorial studies have revealed a strong interplay between physical forcing and biogeochemical cycling [*Murray et al.*, 1995]. Not only do the distinct current systems and alternating water masses dictate the distribution and biomass of the microbial community, but the seasonal occurrence of Kelvin waves and tropical instability waves (TIW) influences the upward vertical flux of nutrients and thus the short-term variability of the phytoplankton community [*Bidigare and Ondrusek*, 1996]. Furthermore, on interannual scales the timing and phase of El Niño-Southern Oscillation (ENSO) affect the extent and strength of the upwelling system as well as the formation and frequency of TIW and Kelvin waves.

Table 5. Microbial Community Characteristics Along 180°[a]

Station	C:chl	% PROK	% POC	AC:HC
8°S	114	47	77	1.7
7°S	66	55	44	1.2
6°S	91	44	56	1.2
5°S	93	41	53	1.3
4°S	80	41	70	1.3
3°S	101	52	n/a	1.3
2°S	100	44	88	1.1
1°S	108	38	73	1.7
0°	100	37	n/a	1.5
1°N	88	35	77	1.5
2°N	57	29	58	0.9
3°N	77	29	70	1.0
4°N	94	34	72	1.5
5°N	64	30	78	0.8
6°N	68	40	54	0.8
7°N	76	43	72	0.8
8°N	85	43	51	0.6

[a]All parameters are integrated to 100 m. C:chl is the ratio of autotrophic carbon to total chlorophyll *a*. % PROK is the percent of total biomass attributed to prokaryotes (HBACT + PRO + SYN), and % POC is the percent of particulate organic carbon (Y. Suzuki, unpublished data) attributed to living microbial biomass. AC:HC represents the ratio of autotrophic to heterotrophic carbon.

[50] The timing of the EBENE cruise was fortuitous in that the equatorial upwelling reaches as far west as the date line only during ENSO cold phases [*Picaut et al.*, 1996]. This provided an unusual opportunity to evaluate the western most reaches of the upwelling zone, particularly as the frequency of ENSO cold phases appears to have decreased since the 1970s [*Trenburth and Hurrell*, 1994]. In addition, the westward extension of the cold tongue resulted in a branch of a TIW eddy that extended further west than usual and passed through our study site. This TIW was marked by an increase in surface temperature (0.2°C), a decrease in surface salinity (0.2) and a shift in current velocity and direction from 20 cm s^{-1} westward to >80 cm s^{-1} southwestward. In addition, a notable decrease in nitrate concentrations from the surface to 90 m was apparent as well as an increase in subsurface ammonium [*Eldin and Rodier*, 2003].

[51] The distribution of Tchl *a* was fairly monotonous throughout the equatorial region from 5°S to 5°N with the only modest enhancement from 50 to 100 m at 0°–1°N. This semi-uniform distribution contrasts with previous results in both the western and the central equatorial Pacific, which showed bimodal distributions of integrated chlorophyll a few degrees of latitude to either side of the equator, reflecting the net growth of larger phytoplankton advected away from the upwelling divergence [*Bidigare and Ondrusek*, 1996] or areas of localized mixing via either upwelling or vertical shear [*Mackey et al.*, 1995, 1997]. The lack of such a distribution at 180°W might have been due, in part, to a weaker upwelling system at this time and less advection to the north and south. More likely, the biomass accumulation centered at 0° was due to the convergence in the meridional component of the SEC at the equator, opposing the transport associated with active upwelling [*Eldin and Rodier*, 2003, Figure 2d].

[52] Unlike chlorophyll, phytoplankton biomass was, in fact, concentrated near the surface in the upwelling region. The increase in C:chl ratios in the equatorial zone and the assymetrical distribution of higher values to the south (Figure 2) are consistent with prior studies [*Chavez et al.*, 1996]. *Chavez et al.* [1996] reported surface ratios of 50–60 north of 5°N, and ratios in the equatorial region and to the south at least twofold higher, even exceeding 200. Maximum surface ratios along the EBENE transect were not as high as found by *Chavez et al.* [1996]; nevertheless, the latitudinal trend was similar. Both C:chl ratios reported here and those of *Chavez et al.* [1996] are significantly higher than the commonly used euphotic zone average of 58 from *Eppley et al.* [1992]. While *Chavez et al.* [1996] attribute the difference to surface ratios versus euphotic zone values, our integrated ratios exceed 58 at all but one station, averaging 100 from 3°S to 0°. The discrepancy almost certainly lies in differences in methodology, as the *Eppley et al.* [1992] ratio was determined from the slope of the regression of chl *a* versus POC.

[53] The elevated C:chl ratios in the more productive equatorial zone are somewhat counterintuitive. We would expect small dominant cells in stratified oligotrophic waters to have reduced chlorophyll per cell as a photoadaptive response to high light levels and a physiological response to low iron concentrations, leading to high C:chl ratios. Conversely, cells in the divergence zone, which represent the location where most "new" iron enters surface waters from the equatorial undercurrent [*Coale et al.*, 1996] should have increased pigment per cell, resulting in lower C:chl ratios. During the IronEx II fertilization for example, this stimulatory effect was seen very clearly as a sharp decline in C:chl from >150 to 70 [*Landry et al.*, 2000b]. Significant decreases in pigment per cell in this region could conceivably account for the unexpected ratios; however, neither FCM-derived red fluorescence per cell of PRO nor spectrofluorometric dv-chl *a* concentrations relative to cell abundance showed any latitudinal trends.

[54] Given the similarities in sizes of the three prokaryote groups (PRO, SYN, HBACT), they should be susceptible to the same suite of grazers and thus their variability and distributions should be related to some extent [*Landry and Kirchman*, 2002]. The bacterial groups all showed greater abundances in the upwelling zone reaching as far south as 5°S, reflecting the asymmetrical distribution of nutrients and in particular, the presence of NH_4 up to the surface [*Eldin and Rodier*, 2003]. The prokaryote abundance maxima at 3°S did not correspond to a distinct physical or chemical signal in the water column, except perhaps that they overlaid subsurface nitrite and ammonium maxima. Abundance of the likely predators of bacteria-sized prey, $\leq$–8-μm protistan grazers, were also locally enhanced at 3°S, and their grazing and remineralization may account, in part, for the ammonium maximum there.

[55] The region of enhanced photosynthetic and heterotrophic biomass between 4° and 5°N (Figures 5 and 9) reflects the boundary between the SEC and the NECC. During ENSO cold phases, both the SEC and the NECC have a greater velocity than normal [*Eldin and Rodier*, 2003], making the frontal boundary between the two currents quite distinct. Also evident at 4°–5°N was a deepening of the thermocline resulting in a 1.5° C temperature anomaly, indicative of strong convergence and consistent with the accumulation of biomass. This is potentially important with regard to export since it appears that the flux of phytodetritus to the equatorial seafloor is associated with the advective accumulation and sinking of large phytoplankton (diatoms) at convergent fronts, rather than bloom events per se [*Smith et al.*, 1996].

[56] Although not as sizable, an analogous enhancement of biomass, attributable mainly to the $\leq$8-μm PEUKS (Figure 5) was found on the southern edge of the SEC. Since velocity of the SEC was only one-half that of its northern counterpart [*Eldin and Rodier*, 2003], conditions favoring the development of a frontal feature were less likely than in the north. This is somewhat in contrast to previous results in the western equatorial Pacific (165°W) in which a strong, permanent convergence was found between the SEC and the SECC [*Radenac and Rodier*, 1996]. In addition, the SECC cut through the SEC with evidence of equatorial waters to the south of the SECC at 8°S, 50–200 m [*Eldin and Rodier*, 2003, Figure 2c]. This intrusion may account for the slight enhancement of PRO, large phytoplankton and the high C:chl ratio at this station.

[57] During EBENE, the advection of the southward branch of a TIW eddy from the northeast resulted in warm, fresh nitrate-impoverished water extending into the upwelling zone and reaching the equator [*Eldin and Rodier*, 2003]. Despite the lower concentrations of nitrate,

phytoplankton biomass and component communities were surprisingly similar to those of the upwelled waters in the southern portion of the divergence zone. Presumably, this returning branch of an anticyclonic eddy was biologically "older" than freshly upwelled waters and represented a more mature microbial community. Such an interpretation would be consistent with the enhancement of grazer abundance and biomass and the inverted trophic structure described previously.

[58] In summary, the distribution and structure of the microbial populations were clearly related to the physical structure of the equatorial region. The equatorial zone was an area of enhanced phytoplankton biomass, whereas heterotrophic biomass dominated in the more mature community of the oligotrophic NECC and in the northern portion of the SEC, influenced by the TIW. C:chl ratios were higher in the divergent zone of the equatorial Pacific and showed distinct latitudinal variations. The convergent zone between the SEC and the NECC was an area of substantial accumulation of biomass, which would likely enhance export flux in this area. Although the general size structure of the microbial community was similar to previous reports with the dominance of small species, the spatial distribution of picophytoplankton varied without obvious causes. The larger phytoplankton community differed with respect to the paucity of small pennate diatoms, the presence of larger forms, and enhanced abundance of large dinoflagellates. These changes in community structure with the physical features of the region and the differences in composition from previous studies imply both spatial and temporal variability in the microbial community that are likely to influence food web interactions and biogeochemical fluxes.

[59] **Acknowledgments.** This study was supported in part by NSF grants OCE-9218152, -9617409, and -9911765 as well as travel and logistical support from the IRD Centre de Noumea. We thank the captain and crew of the N.O. *L'Atalante*, Scott Nunnery, and our shipmates who contributed to our efforts. We especially thank Chief Scientist R. Le Borgne for his leadership and organization and for the opportunity to participate in the EBENE cruise. This paper is contribution number 977 from the U.S. JGOFS Program and number 6247 from the School of Ocean and Earth Science and Technology, University of Hawaii at Manoa, Honolulu, HI, USA.

References

Bidigare, R. R., and M. E. Ondrusek, Spatial and temporal variability of phytoplankton pigment distributions in the central equatorial Pacific Ocean, *Deep Sea Res., Part II*, *43*, 809–832, 1996.

Binder, B. J., S. W. Chisholm, R. J. Olson, S. L. Frankel, and A. Z. Worden, Dynamics of picophytoplankton, ultraphytoplankton and bacteria in the central equatorial Pacific, *Deep Sea Res., Part II*, *43*, 907–932, 1996.

Blanchot, J., and M. Rodier, Picophytoplankton abundance and biomass in the western tropical Pacific Ocean during the 1992 El Niño year: Results from flow cytometry, *Deep Sea Res., Part I*, *43*, 877–895, 1996.

Bockstahler, K. R., and D. W. Coats, Spatial and temporal aspects of mixotrophy in Chesapeake Bay dinoflagellates, *J. Eukaryotic Microbiol.*, *40*, 49–60, 1993.

Brown, S. L., and M. R. Landry, Mesoscale variability in biological community structure and biomass in the Antarctic polar front region at 170°W during austral spring 1997, *J. Geophys. Res.*, *106*, 13,917–13,930, 2001.

Buck, K. R., F. P. Chavez, and L. Campbell, Basin-wide distributions of living carbon components and the inverted trophic pyramid of the central gyre of the North Atlantic Ocean, summer 1993, *Aquat. Microbial Ecol.*, *10*, 283–298, 1996.

Calbet, A., and M. R. Landry, Mesozooplankton influences on the microbial food web: Direct and indirect trophic interactions in the oligotrophic open-ocean, *Limnol. Oceanogr.*, *44*, 1370–1380, 1999.

Campbell, L., H. A. Nolla, and D. Vaulot, The importance of *Prochlorococcus* to community structure in the central North Pacific Ocean, *Limnol. Oceanogr.*, *39*, 954–961, 1994.

Chavez, F. P., K. R. Buck, S. K. Service, J. Newton, and R. T. Barber, Phytoplankton variability in the central and eastern tropical Pacific, *Deep Sea Res., Part II*, *43*, 835–870, 1996.

Chisholm, S. W., R. J. Olson, E. R. Zettler, R. Goericke, J. B. Waterbury, and N. A. Welschmeyer, A novel free-living prochlorophyte abundant in the oceanic euphotic zone, *Nature*, *334*, 340–343, 1988.

Chisholm, S. W., S. L. Frankel, R. Goericke, R. J. Olson, B. Palenik, J. B. Waterbury, L. West-Johnsrud, and E. Zettler, *Prochlorococcus marinus* nov. gen. nov. sp.: And oxyophototrophic marine prokaryote containing divinyl chlorophyll *a* and *b*, *Arch. Microbiol*, *157*, 297–300, 1992.

Cho, B. C., and F. Azam, Biogeochemical significance of bacterial biomass in the ocean's euphotic zone, *Mar. Ecol. Prog. Ser.*, *63*, 253–259, 1990.

Coale, K. H., et al., A massive phytoplankton bloom induced by an ecosystem-scale iron fertilization experiment in the equatorial Pacific Ocean, *Nature*, *383*, 495–501, 1996.

Cole, J. J., S. Findlay, and M. L. Pace, Bacterial production in fresh and saltwater ecosystems: A cross-system overview, *Mar. Ecol. Prog. Ser.*, *43*, 1–10, 1988.

Eldin, G., and M. Rodier, Ocean physics and nutrient fields along 180° during an El Niño-Southern Oscillation cold phase, *J. Geophys. Res.*, *108*(C12), 8137, doi:10.1029/2000JC000746, 2003.

Eppley, R. W., F. M. H. Reid, and J. D. H. Strickland, Estimates of phytoplankton crop size, growth rate, and primary production, in *The Ecology of the Plankton off La Jolla California in the Period April Through September, 1967*, edited by H. J. D. Strickland, *Bull. Scripps Inst. Oceanogr.*, *17*, 33–42, 1970.

Eppley, R. W., F. P. Chavez, and R. T. Barber, Standing stocks of particulate carbon and nitrogen in the equatorial Pacific at 150°W, *J. Geophys. Res.*, *97*, 655–661, 1992.

Fuhrman, J. A., T. D. Sleeter, C. A. Carlson, and L. M. Proctor, Dominance of bacterial biomass in the Sargasso Sea and its ecological implications, *Mar. Ecol. Prog. Ser.*, *57*, 207–217, 1989.

Garrison, D. L., et al., Microbial food web structure in the Arabian Sea: A US JGOFS study, *Deep Sea Res., Part II*, *47*, 1387–1422, 2000.

Hasle, G. R., A quantitative study of phytoplankton from the equatorial Pacific, *Deep Sea Res.*, *6*, 38–59, 1959.

Iriarte, J. L., and G. A. Fryxell, Micro-phytoplankton at the equatorial Pacific (140°W) during the JGOFS EqPac time series studies: March to April and October 1992, *Deep Sea Res., Part*, *42*, 559–584, 1995.

Ishizaka, J., K. Harada, K. Ishikawa, H. Kiyosawa, H. Furusawa, Y. Watanabe, H. Ishida, K. Suzuki, N. Handa, and M. Takahashi, Size and taxonomic plankton community structure and carbon flow at the equator, 175°E during 1990–1994, *Deep Sea Res., Part II*, *44*, 1927–1950, 1997.

Kaczmarska, I., and G. A. Fryxell, Micro-phytoplankton of the equatorial Pacific: 140°W meridional transect during the 1992 El Niño, *Deep Sea Res., Part II*, *42*, 535–558, 1995.

Landry, M. R., and D. L. Kirchman, Microbial community structure and variability in the tropical Pacific, *Deep Sea Res., Part II*, *49*, 2669–2693, 2002.

Landry, M. R., J. Kirshtein, and J. Constantinou, Abundances and distributions of picoplankton populations in the central equatorial Pacific from 12°S to 12°N, 140°W, *Deep Sea Res., Part II*, *43*, 871–890, 1996.

Landry, M. R., et al., Iron and grazing constraints on primary production in the central equatorial Pacific: An EqPac synthesis, *Limnol. Oceanogr.*, *42*, 405–418, 1997.

Landry, M. R., J. Constantinou, M. Latasa, S. L. Brown, R. R. Bidigare, and M. E. Ondrusek, Biological response to iron fertilization in the eastern equatorial Pacific (IronEx II). III., Dynamics of phytoplankton growth and microzooplankton grazing, *Mar. Ecol. Prog. Ser.*, *201*, 57–72, 2000a.

Landry, M. R., M. E. Ondrusek, S. J. Tanner, S. L. Brown, J. Constantinou, R. R. Bidigare, K. H. Coale, and S. Fitzwater, Biological response to iron fertilization in the eastern equatorial Pacific (IronEx II). I., Microplankton community abundances and biomass, *Mar. Ecol. Prog. Ser.*, *201*, 27–42, 2000b.

Landry, M. R., S. L. Brown, J. Neveux, C. Dupouy, J. Blanchot, S. Christensen, and R. R. Bidigare, Phytoplankton growth and microzooplankton grazing in high-nutrient, low-chlorophyll waters of the equatorial Pacific: Community and taxon-specific rate assessments from pigment and flow cytometric analyses, *J. Geophys. Res.*, *108*(C12), 8142, doi:10.1029/2000JC000744, 2003.

Lantoine, F., and J. Neveux, Spatial and seasonal variations in abundance and spectral characteristics of phycoerythrins in the tropical northeastern Atlantic Ocean, *Deep Sea Res., Part I*, *44*, 223–246, 1997.

Latasa, M., M. R. Landry, L. Schluter, and R. R. Bidigare, Pigment-specific growth and grazing rates of phytoplankton in the central equatorial Pacific, *Limnol. Oceanogr.*, *42*, 289–298, 1997.

Le Borgne, R., G. Champalbert, and R. Gaudy, Mesozooplankton biomass and composition in the equatorial Pacific along 180°, *J. Geophys. Res.*, *108*(C12), 8143, doi:10.1029/2000JC000745, 2003.

Le Bouteiller, A., J. Blanchot, and M. Rodier, Size distribution patterns of phytoplankton in the western Pacific: Towards a generalization for the tropical open ocean, *Deep Sea Res., Part A*, *39*, 805–823, 1992.

Leynaert, A., P. Treguer, C. Lancelot, and M. Rodier, Silicon limitation in the equatorial Pacific: Evidence from Si uptake kinetics studies, *Deep Sea Res., Part I*, *48*, 639–660, 2001.

Li, A., D. K. Stoecker, D. W. Coats, and E. J. Adams, Ingestion of fluorescently labeled and phycoerythrin-containing prey by mixotrophic dinoflagellates, *Aquat. Microbial Ecol.*, *10*, 139–147, 1996.

Mackey, D. J., J. Parslow, H. W. Higgins, F. B. Griffiths, and J. E. O'Sullivan, Plankton productivity and biomass in the western equatorial Pacific: Biological and physical controls, *Deep Sea Res., Part II*, *42*, 499–533, 1995.

Mackey, D. J., J. S. Parslow, F. B. Griffiths, H. W. Higgins, and B. Tilbrook, Phytoplankton productivity and the carbon cycle in the western equatorial Pacific under El Niño and non-El Niño conditions, *Deep Sea Res., Part II*, *44*, 1951–1978, 1997.

Mackey, D. J., J. Blanchot, H. W. Higgins, and J. Neveux, Phytoplankton abundances and community structure in the equatorial Pacific, *Deep Sea Res., Part II*, *49*, 2561–2582, 2002.

Monger, B. C., and M. R. Landry, Flow cytometric analysis of marine bacteria with Hoechst 33342, *Appl. Environ. Microbiol.*, *59*, 905–911, 1993.

Murray, J. W., E. Johnson, and C. Garside, A U.S. JGOFS process study in the equatorial Pacific (EqPac): Introduction, *Deep Sea Res., Part II*, *42*, 275–294, 1995.

Neveux, J., and F. Lantoine, Spectrofluorometric assay of chlorophylls and phaeopigments using the least squares approximation technique, *Deep Sea Res., Part I*, *40*, 1747–1765, 1993.

Neveux, J., F. Lantoine, D. Vaulot, D. Marie, and J. Blanchot, Phycoerythrins in the southern tropical and equatorial Pacific Ocean: Evidence for new cyanobacterial types, *J. Geophys. Res.*, *104*, 3311–3322, 1999.

Neveux, J., C. Dupouy, J. Blanchot, A. Le Bouteiller, M. R. Landry, and S. L. Brown, Diel dynamics of chlorophylls in high-nutrient, low-chlorophyll waters of the equatorial Pacific (180°): Interactions of growth, grazing, physiological responses, and mixing, *J. Geophys. Res.*, *108*(C12), 8140, doi:10.1029/2000JC000747, 2003.

Olson, R. J., S. W. Chisholm, E. R. Zettler, M. A. Altabet, and J. A. Dusenberry, Spatial and temporal distributions of prochlorophyte picoplankton in the North Atlantic Ocean, *Deep Sea Res., Part I*, *37*, 1033–1051, 1990a.

Olson, R. J., E. R. Zettler, E. V. Armbrust, and S. W. Chisholm, Pigment, size and distribution of Synechococcus in the North Atlantic and Pacific Oceans, *Limnol. Oceanogr.*, *35*, 45–58, 1990b.

Picaut, J., M. Ioualalen, C. Menkes, T. Delcroix, and M. J. McPhaden, Mechanisms of the zonal displacement of the Pacific warm pool: Implications for ENSO, *Science*, *274*, 1486–1489, 1996.

Porter, K. G., Phagotrophic phytoflagellates in microbial food webs, *Hydrobiologia*, *159*, 89–97, 1988.

Radenac, M.-H., and M. Rodier, Nitrate and chlorophyll distributions in relation to thermohaline and current structures in the western tropical Pacific during 1985–1989, *Deep Sea Res., Part II*, *43*, 725–752, 1996.

Sanders, R. W., and K. G. Porter, Phagotrophic phytoflagellates, *Adv. Microbial Ecol*, *10*, 167–192, 1988.

Semina, H. J., The size of phytoplankton cells in the Pacific Ocean, *Hydrobiologie*, *57*, 177–205, 1972.

Shalapyonok, A., R. J. Olson, and L. S. Shalapyonok, Arabian Sea phytoplankton during the southwest and northeast monsoons 1995: Composition, size structure, and biomass from individual cell properties measured by flow cytometry, *Deep Sea Res., Part II*, *48*, 1231–1261, 2001.

Sherr, E. B., and B. F. Sherr, Preservation and storage of samples for enumeration of heterotrophic protists, in *Handbook of Methods in Aquatic Microbial Ecology*, edited by P. K. Kemp et al., pp. 207–212, CRC Press Boca Raton, Fla., 1993.

Smith, C. R., D. J. Hoover, S. E. Doan, R. H. Pope, D. J. Demaster, F. C. Dobbs, and M. A. Altabet, Phytodetritus at the abyssal sea floor across 10° of latitude in the central equatorial Pacific, *Deep Sea Res., Part II*, *43*, 1309–1338, 1996.

Stoecker, D. K., D. E. Gustafson, and P. G. Verity, Micro- and mesoprotozooplankton at 140°W in the equatorial Pacific: Heterotrophs and mixotrophs, *Aquat. Microbial Ecol.*, *10*, 273–282, 1996.

Strathmann, R. R., Estimating the organic carbon content of phytoplankton from cell volume or plasma volume, *Limnol. Oceanogr.*, *36*, 50–63, 1967.

Trenburth, K. E., and J. W. Hurrell, Decadal atmosphere-ocean variations in the Pacific, *Clim. Dyn.*, *9*, 303–319, 1994.

Verity, P. G., D. K. Stoecker, M. E. Sieracki, and J. R. Nelson, Microzooplankton grazing of primary production at 140°W in the equatorial Pacific, *Deep Sea Res., Part II*, *43*, 1227–1255, 1996.

Vors, N., K. R. Buck, F. P. Chavez, W. Eikrem, L. E. Hansen, J. B. Ostergaard, and H. A. Thomsen, Nanoplankton of the equatorial Pacific with emphasis on the heterotrophic protists, *Deep Sea Res.*, *42*, 585–602, 1995.

Wyman, M., An in vivo method for the estimation of phycoerythrin concentrations in marine cyanobacteria (*Synechococcus* spp.), *Limnol. Oceanogr.*, *37*, 1300–1306, 1992.

S. L. Brown and M. R. Landry, Department of Oceanography, University of Hawaii at Manoa, 1000 Pope Rd., Honolulu, HI 96822, USA. (sbrown@soest.hawaii.edu)

C. Dupouy, Laboratoire d'Océanographie Dynamique et de Climatologie (LODYC), Institut de Recherche pour le Développment (IRD), Université Pierre et Marie Curie, 4 place Jussieu, Tour 14-15, boite 100, 75252- Paris, France.

J. Neveux, Observatoire Océanologique de Banyuls, Laboratoire Arago (UMR 7621), BP 44, 66651- Banyuls sur Mer Cedex, France.

Brown S.L., Landry M.R., Neveux J., Dupouy Cécile. (2003).

Microbial community abundance and biomass along a 180° transect in the equatorial Pacific during an El Nino-Southern Oscillation cold phase.

In : A JGOFS investigation of plankton variability and trophic interactions in the central equatorial Pacific (EBENE).

Journal of Geophysical Reasearch, 108 (C12), 4-1 - 4-15. ISSN 0148-0227